J Appl Electrochem (2014) 44:893–902
DOI 10.1007/s10800-014-0706-y

RESEARCH ARTICLE

Enhanced electrooxidation of methanol, ethylene glycol, glycerol, and xylitol over a polypyrrole/manganese oxyhydroxide/palladium nanocomposite electrode

Ramanujam Kannan · Ae Rhan Kim · Dong Jin Yoo

Received: 21 February 2014 / Accepted: 10 June 2014 / Published online: 16 July 2014

Abstract A small quantity of palladium metal (Pd, 5 wt%) nanoparticles supported by a polypyrrole/manganese oxyhydroxide (PPy/MOH) nanocomposite was developed and investigated as an electrocatalyst for the alcohol electrooxidation reaction in alkaline media. In voltammetric studies, the PPy/MOH/Pd catalyst, compared to C/Pd, exhibited improved electrocatalytic activity for methanol electrooxidation. The peak current density ratios (j^f/j^b) for the C/Pd and PPy/MOH/Pd nanocomposite electrodes were 0.67 and 2.43, respectively, indicating that the PPy/MOH/Pd nanocomposite electrode was much more resistant to catalytic poisoning. The electrooxidation of ethylene glycol (EG), glycerol, and xylitol was also tested using the PPy/MOH/Pd nanocomposite electrode. Among these alcohol electrooxidations, that of EG exhibited the maximum power density of 430 mA cm^{-2}. The intermediates formed during the electrooxidation reactions were removed by increasing the upper sweep potential from +0.2 to +1.0 V. The catalytic performance of the PPy/MOH nanocomposite is discussed in detail. The study results demonstrate that PPy/MOH acts as a superior catalytic supporting material for alcohol electrooxidation reactions in alkaline media.

Keywords Manganese oxyhydroxide · Polypyrrole · Palladium · Electrooxidation · Electrocatalyst

R. Kannan · D. J. Yoo (✉)
R&D Education Center for Specialized Graduate School of Hydrogen and Fuel Cells Engineering, Chonbuk National University, Jeollabuk–do 561-756, Korea
e-mail: djyoo@jbnu.ac.kr

R. Kannan · D. J. Yoo
Graduate School, Department of Energy Storage/Conversion Engineering, Hydrogen and Fuel Cell Research Center, Chonbuk National University, Jeollabuk–do 561-756, Korea

A. R. Kim
Department of Chemistry, Chonbuk National University, Jeollabuk–do 561-756, Korea

1 Introduction

Direct alcohol fuel cells (DAFC) are attractive as power sources for portable applications. Alcohols such as methanol, ethanol, ethylene glycol (EG), and glycerol have been studied extensively for their potential use as fuels. Compared to hydrogen, these alcohols have higher volumetric energy density, and their storage and transport are also much easier. However, the fuel cell (FC) kinetics of alcohol-fuelled FCs are comparatively lower than that of hydrogen-fuelled FCs. FC catalysts have been identified as major contributors to the kinetics. Research on improving DAFC kinetics is focusing on the design of more efficient electrocatalyst [1–11].

Platinum (Pt) and Pt-based alloys are the most commonly used electrocatalyst for DAFCs, because they offer high catalytic activity, chemical stability, high current density, and superior work functions. However, the use of Pt–based catalyst has been restricted due to their high cost, the limited supply of Pt, and the high adsorption of reaction intermediates by these catalysts that lead to reduced activity [1–9]. Much effort has been applied toward overcoming these problems with the goal of developing less expensive anode with significant catalytic activity. This can be achieved by replacing Pt with another metal catalyst and/or by supporting the metal catalyst on a suitable material. Pd is a promising electrocatalytic substitute for Pt, because it is less expensive and exhibits similar

electrocatalytic activity [3–5]. Supported metal catalysts offer improved stability and higher catalytic activity than the unsupported catalyst [1–4]. A good interaction between the catalyst and support not only improves the catalytic activity but can also enhance the catalyst's performance and durability by reducing catalyst poisoning by the intermediates [1–7].

Conventionally, conductive carbon materials such as carbon black, Vulcan XC, and Ketjen black are used as the support materials for FC electrocatalyst. On the other hand, carbon corrosion occurs in dynamic-load operation, causing the catalyst to become electronically isolated and leading to poor catalyst utilization. It is impossible to completely prevent carbon corrosion. Consequently, to address this issue, non-carbon based support materials have been used [2–4]. Among the various support materials [9–26], metal oxides play an important role, because they can be prepared easily in the desired sizes and shapes, and they are cost-effective to produce and are non-toxic. Recently, CeO_2 [17], NiO [17], Mn_3O_4 [17, 18], TiO_2 [19], MnO_2 [20–22], MnOOH [23–25], and SnO_2 [26] have been used as support materials for metal catalysts for polymer electrolyte membrane FCs.

In recent years, manganese oxide-based (MnOx) materials have attracted more attention and have been widely used in electrochemical supercapacitors. Recent studies show that the MnOx materials act as co-catalyst, and the improved electrooxidation reaction is achieved through reduced interference with CO [19–21]. On the other hand, the poor electrical conductivity of MnOx restricts its practical use as an electrode material. To overcome this problem, a number of composites of MnOx with carbon, carbon nanotubes, graphene, and conducting polymers have been studied [16, 27]. Among these conducting polymer composites show enhanced catalytic activity. The use of conducting polymers enhances the properties of the interface between electrode and electrolyte, and facilitates the electrocatalytic activity [28]. In addition to that, polymeric matrix enhances the conductivity and acts a co-catalyst for the oxidation of intermediate poisonous species [3, 15]. The polymeric network facilitates the electrical conduction, thereby the electrical conductivity of MOH is improved. In addition to that, the MOH-PPy composite is synthesized with expectation of (MOH) Mn–N (PPy) interaction creates active catalytic site to enhance the electrocatalytic activity. To the best of our knowledge, few studies have investigated the use of metal oxide/conducting polymer composites as a support material for a metal catalyst. Recently, Wei et al. [27] studied Pt nanoparticles supported on a manganese oxide-poly(3,4-ethylenedioxythiophene)-carbon nanotubes composite for enhancing methanol electrooxidation. Recently, our group reported the enhanced electrooxidation of methanol and ethanol over Pd nanoparticles supported on a polyaniline/MnO_2 nanocomposite [16].

In the present study, a ternary electrocatalyst composed of Pd nanoparticles on PPy/MOH was developed for the efficient electrooxidation of methanol, EG, glycerol, and xylitol in alkaline media. The MOH functions as a co-catalyst, helping to extract active oxygen from the electrolyte. The results indicate that the PPy/MOH support material shows enhanced catalytic activity, and the intermediates were removed by increasing the upper scanning potential.

2 Experimental

2.1 Materials

Potassium permanganate, pyrrole, ammonium peroxodisulphate, hydrogen peroxide (30 % v/v), acetic acid, sodium acetate, hydrochloric acid, potassium hydroxide, palladium acetate, formaldehyde, methanol, EG, glycerol, xylitol, and ethanol were received from Merck company, India. Vulcan XC carbon was obtained from Cabot Corp. India. All the chemicals were of analytical grade and were used without further purification.

2.2 Characterizations

The prepared MOH, PPy/MOH, and PPy/MOH/Pd nanocomposite were characterized by powder X-ray diffraction (XRD; Shimadzu Lab X–6000), energy dispersive X-ray analysis (EDX; INSTA-FET, Oxford Instruments), and transmission electron microscope (TEM; JEOL, JSM 2100). Electrochemical studies using the nanocomposite were carried out by a CHI 660C electrochemical workstation (CH Instruments) equipped with a three-electrode system and a software control system.

2.3 Preparation of MOH and PPy/MOH nanocomposite

MOH was prepared by the following hydrothermal process. Hydrogen peroxide (40 mL) and an acetate buffer (a mixture of 5 mL acetic acid and 5 g sodium acetate) were added dropwise to an aqueous solution of potassium permanganate (6.5 g in 200 mL). After complete addition to the solution, the resulting gel was refluxed at 70 °C for 2 h. The product was separated by centrifugation, washed several times with deionized (DI) water, and then dried in a hot air oven at 105 °C. The resulting sample was designated as MOH and used for further study.

About 1 mL of pyrrole was added to 10 mL of DI water, followed by the addition of a few drops of diluted hydrochloric acid. After 10 min, 100 mg of MOH was added to

this solution and stirred for 30 min. Then, 2–3 mL of aqueous ammonium peroxodisulphate solution (0.1 M) was added with constant stirring. After 1 h, the precipitate was separated by centrifugation, washed, and then dried in an oven at 80 °C for 12 h. This product was designated as PPy/MOH composite. Pure PPy was prepared by the same method except without the addition of MOH.

2.4 Preparation of PPy/MOH/Pd nanocomposite

The PPy/MOH/Pd nanocomposite was synthesized by in situ reduction method. After 95 mg of PPy/MOH composite was dispersed in DI water, aqueous palladium acetate solution (0.5 mM) was then added to achieve 5 wt% Pd (5 mg) in the catalyst. Two milliliters of formaldehyde solution were added dropwise to this mixture at room temperature and stirred for 2 h. The resulting solid product was then filtered, washed with DI water, and dried at 80 °C. This solid catalyst was designated as PPy/MOH/Pd nanocomposite. The PPy/Pd nanocomposite was prepared by the same method except without the addition of MOH.

2.5 Fabrication of PPy/MOH/Pd electrode and electrochemical measurements

A glassy carbon (GC) electrode (3 mm dia., CH Instruments) was polished using 0.05 μm alumina powder. The nanocomposite-modified GC, Pt, and standard calomel electrodes were used as working, counter, and reference electrodes, respectively. Unless otherwise specified, all cyclic voltammograms (CVs) were measured at a scan speed of 50 mV s^{-1}, and DI water was used for each experiment.

The modified electrode was prepared by the drop-casting method. The PPy/MOH/Pd nanocomposite was ultrasonically dispersed in Nafion solution (0.5 % in ethanol), and the resultant colloidal solution was dropped on the GC electrode and allowed to dry in a vacuum. As a comparison electrode, a Pd-dispersed carbon powder (C, Vulcan XC-72) modified GC electrode was prepared by the same method described above. To avoid interference by oxygen, the experiments were performed in N_2–saturated conditions.

3 Results and discussion

3.1 Physical characterizations of the PPy/MOH/Pd nanocomposite

Figure 1 shows the powder XRD profiles for MOH, PPy/MOH, and the PPy/MOH/Pd nanocomposite. In Fig. 1a, the peaks (2θ) at 19.2° (102), 21.5° (401), 25.1° (222), and 28.9° (511) indicate, the formation of hydrated MOH

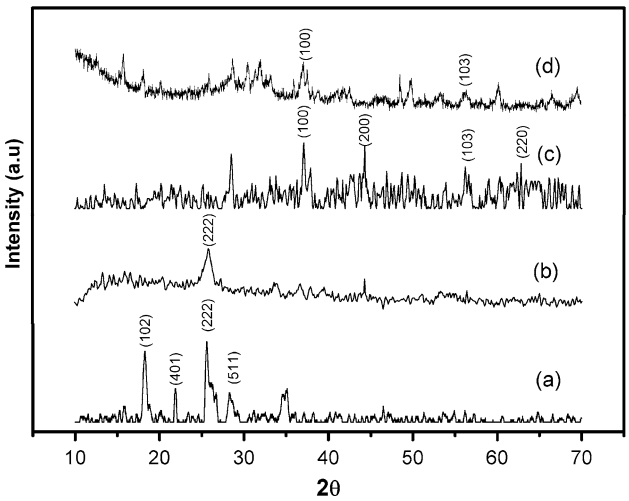

Fig. 1 Powder XRD spectra of (**a**) MOH, (**b**) MOH/Pd, (**c**) PPy/MOH/Pd and (**d**) C/Pd

(γ-$Mn(O,OH)_2$, JCPDS 170510). Due to the hydration of the material, an MOH peak that would normally appear in 34.1° was instead observed at 34.8°. The characteristic peak for MOH was observed in 25.1° in PPy/MOH and other peaks were diminished, indicating that the MOH material was highly dispersed within the polymer. The presence of Pd nanoparticles on the PPy/MOH nanocomposite was confirmed through the appearance of new peaks at 37.3° (100-JCPDS #720710), 44.8° (200-JCPDS #870641), 56.3° (103-JCPDS #720710), and 64.8° (220-JCPDS #870641). The XRD pattern of C/Pd shows the number of peaks, the characteristic Pd (100) and Pd (103) are observed in 37.3° and 55.8° respectively (Fig. 1d).

The TEM micrographs (Fig. 2) show the surface morphology of the MOH, PPy/MOH, and PPy/MOH/Pd nanocomposite samples. Figure 2a reveals MOH nanorods of uniform size and with a width and length of about 50 nm and 800–1,000 nm, respectively. In the PPy/MOH composite, the MOH retains its nanorod structure and is uniformly distributed in the PPy matrix (Fig. 2b). The Pd nanoparticles dispersed on the PPy/MOH nanocomposite are shown in Fig. 2c, d. The elemental analysis spectrum for PPy/MOH/Pd is shown in Fig. 3, and reveals the presence of Pd (about 4.7 wt%) in the PPy/MOH/Pd nanocomposite, as well as Mn and O.

3.2 Cyclic voltammograms for PPy/MOH/Pd nanocomposite in alkaline solution

Figure 4(A) shows the CV recorded for the C/Pd, MOH/Pd and PPy/MOH/Pd nanocomposite electrode in the 1 M KOH solution. At PPy/MOH/Pd nanocomposite electrode, as soon as the forward scanning starts, desorption of

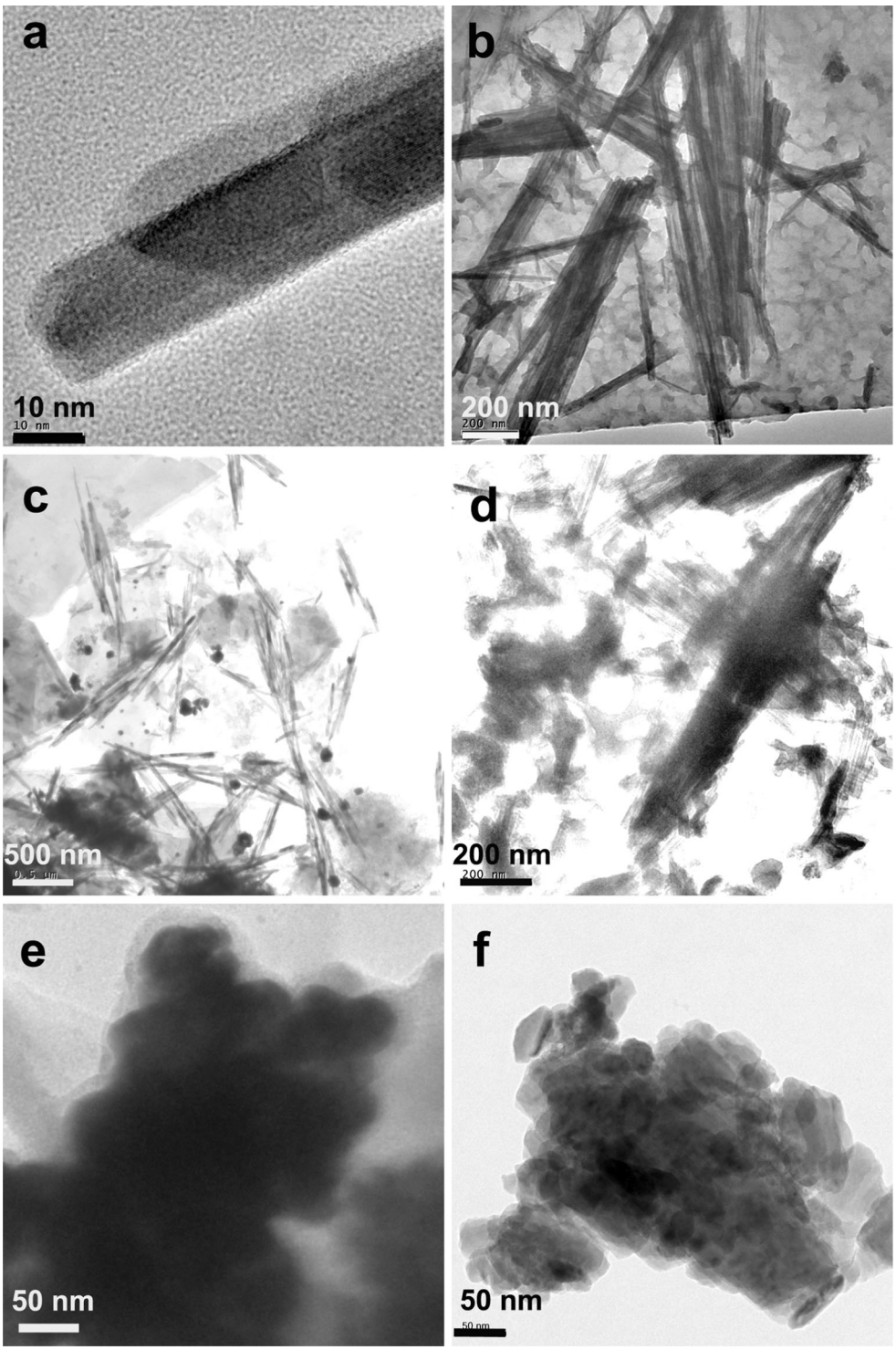

Fig. 2 TEM images of **a** MOH, **b** MOH in the PPy nanocomposite matrix, **c–e** Pd nanoparticles dispersed in the PPy/MOH nanocomposite matrix and **f** Pd nanoparticles over the carbon

hydrogen began vigorously and reached a maximum at −0.91 V. The hydrogen desorption began to decrease at Ep = −0.74 V and stabilized at Ep = −0.63 V (peak 1). The adsorption of OH^- ions started at −0.63 V (peak 2). Subsequently, the formation of a PdO layer started at −0.3 V, with a corresponding increase in current intensity up to +0.2 V (peak 3). During the reverse scan, the PdO layer was reduced in the region between −0.1 and −0.5 V

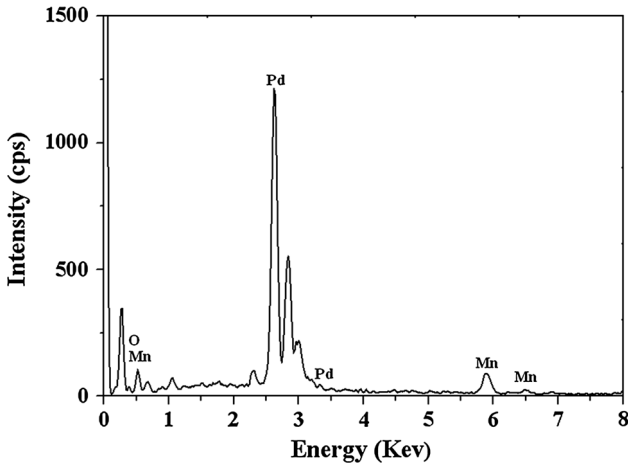

Fig. 3 EDX spectrum of PPy/MOH/Pd nanocomposite

(Ep = −0.4 V, peak 4). The cathodic peak observed at −0.88 V was attributed to the adsorption of hydrogen on the surface of the electrode (Fig. 4(A)c) [29].

$$\text{Peak 1}\quad \text{Pd} - \text{H}_{\text{abs/ads}} + \text{OH}^- \rightleftarrows \text{Pd} + \text{H}_2\text{O} + \text{e}^- \tag{1}$$

$$\text{Peak 2}\quad \text{Pd} + \text{OH}^- \rightleftarrows \text{Pd} - \text{OH}_{\text{ads}} + \text{e}^- \tag{2}$$

$$\text{Peak 3}\quad \text{Pd} - \text{OH}_{\text{ads}} \rightleftarrows \text{PdO} + \text{H}_2\text{O} + \text{e}^- \tag{3}$$

$$\text{Peak 4}\quad \text{PdO} + \text{H}_2\text{O} + \text{e}^- \rightleftarrows \text{Pd} + 2\text{OH}^- \tag{4}$$

In the C/Pd electrode (Fig. 4(A)a), peaks 1, 2, 3, and 4 were observed at −0.88, −0.36, −0.21, and −0.4 V, respectively, with peak currents less than those of the PPy/MOH/Pd electrode. The electrochemical active surface area of PPy/MOH/Pd and C/Pd electrodes was 19.0 and 3.2 $m^2\ g^{-1}$, respectively, and was calculated based on the PdO reduction peak current [30]. The Pd nanoparticles encapsulated in polymer and MOH matrix, hence the electrochemical active surface area for PPy/Pd and MOH/Pd is reduced (1.4 and 0.8 $m^2\ g^{-1}$, respectively). PPy/MOH provided a superior platform for Pd nanoparticles over C, so that more active catalytic sites were available for the reaction. These results clearly demonstrated the marked influence of the supporting material PPy/MOH on the electrochemical activity.

3.3 Electrooxidation of alcohols at the PPy/MOH/Pd nanocomposite electrode

Figure 4B shows the CV of the PPy/MOH/Pd nanocomposite electrode in 1 M KOH/1 M CH_3OH, which demonstrates that the hydrogen desorption/sorption region (−0.9 to −0.7 V) was significantly suppressed in the presence of the CH_3OH/KOH solution. The suppression of this peak was attributed to the dissociative adsorption of the methanol starting in the low potential region [Eqs. (5), (6)]. The methanol oxidation reaction (MOR) started at −0.7 V and the anodic oxidation peak (O^f) occurred in the region −0.35 to −0.08 V, with Ep = −0.2 V. During the backward sweep, the oxidation peak (O^b) appeared in the region −0.29 to −0.5 V with Ep = −0.34 V.

The general mechanistic pathway for MOR at the surface of the Pd electrode is as follows [10, 11].

$$\text{Pd} + \text{OH}^- \rightarrow \text{Pd} - \text{OH} \tag{5}$$

$$\text{Pd} + \text{CH}_3\text{OH} \rightarrow \text{Pd} - (\text{CH}_3\text{OH})_{\text{ads}} \tag{6}$$

$$\text{Pd} - (\text{CH}_3\text{OH})_{\text{ads}} + \text{Pd} - \text{OH} \rightarrow \text{Pd} - (\text{CH}_3\text{O})_{\text{ads}} + \text{Pd} + \text{H}_2\text{O} \tag{7}$$

$$\text{Pd} - (\text{CH}_3\text{O})_{\text{ads}} + \text{Pd} - (\text{OH})_{\text{ads}} \rightarrow \text{Pd}_2 - (\text{CH}_2\text{O})_{\text{ads}} + \text{H}_2\text{O} \tag{8}$$

$$\text{Pd}_2 - (\text{CH}_2\text{O})_{\text{ads}} + \text{Pd} - (\text{OH})_{\text{ads}} \rightarrow \text{Pd}_3 - (\text{CHO})_{\text{ads}} + \text{H}_2\text{O} \tag{9}$$

$$\text{Pd}_3 - (\text{CHO})_{\text{ads}} + \text{Pd} - (\text{OH})_{\text{ads}} \rightarrow \text{Pd}_2 - (\text{CO})_{\text{ads}} + 2\text{Pd} + \text{H}_2\text{O} \tag{10}$$

$$\text{Pd}_2 - (\text{CO})_{\text{ads}} + \text{Pd} - (\text{OH})_{\text{ads}} \rightarrow \text{Pd} - \text{COOH} + 2\text{Pd} \tag{11}$$

$$\text{Pd} - \text{COOH} + \text{Pd} - (\text{OH})_{\text{ads}} \rightarrow 2\text{Pd} + \text{CO}_2 \uparrow + \text{H}_2\text{O} \tag{12}$$

The ratio of the forward sweep peak current density (j_f) to the backward sweep current density (j_b) can be used to determine the tolerance limit of the catalyst. A high j_f/j_b ratio indicates that the oxidation of methanol to carbon dioxide is favorable [16–19]. From Fig. 4b, the qualitative analysis of the voltammograms, the j_f/j_b ratio for the C/Pd and PPy/MOH/Pd nanocomposite electrodes was calculated to be 0.67 and 2.43, respectively. This indicates that the PPy/MOH/Pd electrode was highly active against the poisoning effects of the intermediates compared to the C/Pd electrode. To verify the superiority of the PPy/MOH/Pd nanocomposite electrode, the j_f/j_b ratios for the PPy/Pd and MOH/Pd electrodes were also tested and compared. Table 1 shows that the PPy/MOH/Pd electrode exhibited higher tolerance to intermediates compared to the C/Pd, MOH/Pd, and PPy/Pd electrodes. The MOH/Pd electrode exhibited a minimal peak current of 2 mA cm^{-2}, which we attributed to the poorly conducting nature of the MOH support material. This result highlights the motivation for developing the conductive polymer PPy/MOH: the polymeric film (PPy) offers an extensive network of conductive paths, thereby facilitating the electrooxidation reaction.

Further tests were carried out on the PPy/MOH/Pd nanocomposite electrode, using different alcohols in the electrooxidation reaction: EG, glycerol and xylitol (Fig. 4C). Among them, the EG oxidation reaction (EOR) exhibited a high peak current response, and the xylitol oxidation reaction (XOR) exhibited high tolerance toward

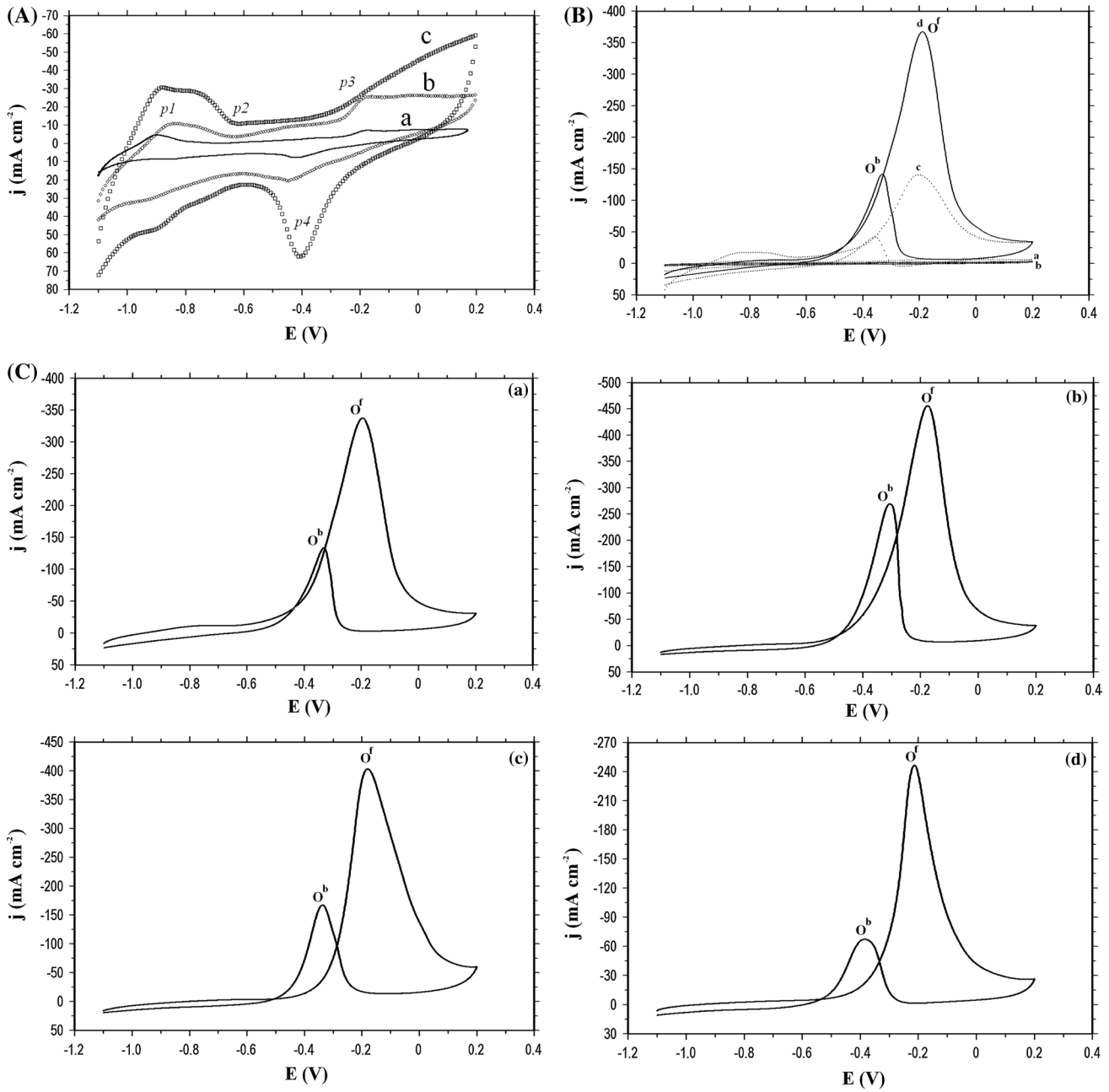

Fig. 4 **A** CVs of (*a*) C/Pd, (*b*) MOH/Pd and (*c*) PPy/MOH/Pd electrodes in 1 M KOH; **B** CVs for the electrooxidation of methanol at (*a*) C/Pd, (*b*) MOH/Pd, (*c*) PPy/Pd, and (*d*) PPy/MOH/Pd nanocomposite electrodes in 1 M KOH/1 M CH_3OH solution; and **C** CVs for the electrooxidation of (*a*) methanol, (*b*) ethylene glycol (EG), (*c*) glycerol, and (*d*) xylitol on PPy/MOH/Pd nanocomposite electrode

poisoning intermediates. The electrooxidation current for GOR and XOR is expected to be higher than methanol and EG, but comparatively both GOR and XOR exhibits lower peak current. We presumed that the bulky nature of the fuels (glycerol and xylitol) and their by-products retards the further oxidation, hence, the peak current is less than the EGOR. The corresponding O^f, $j_{f,}$ O^b, j_b, and j_f/j_b ratios are shown in Table 2. The catalytic tolerance of the PPy/MOH/Pd nanocomposite electrode in the electrooxidation of alcohols decreased in the order of xylitol > methanol > glycol > EG. However, the complete removal of the intermediates remains a challenging problem.

3.4 Possible removal of catalyst poisoning intermediates

During MOR, the formation of catalyst-poisonous intermediate compounds such as Pd–CO_{ads} is the major

Table 1 Comparison of E_f, E_b, and j_f/j_b ratios for the methanol electrooxidation reaction over different electrodes

S. no.	Electrode[a]	O^f (*E*p)	j_f (mA cm^{-2})	O^b (*E*p)	j_b (mA cm^{-2})	j_f/j_b
1	C/Pd	−0.19	2	−0.39	3	0.67
2	MOH/Pd	−0.21	2	–	–	–
3	PPy/Pd	−0.22	91	−0.34	40	2.25
4	PPy/MOH/Pd	−0.20	365	−0.34	150	2.43

[a] 0.2 mg of Pd in the catalyst

Table 2 Comparison of j_f/j_b ratios for the electrooxidation of alcohols over a PPy/MOH/Pd nanocomposite electrode in an alkaline medium

S. no.	Alcohol	PPy/MOH/Pd nanocomposite electrode				
		E_f	j_f	E_b	j_b	j_f/j_b
1	Methanol	+0.20	365	−0.34	150	2.43
2	Ethylene glycol	+0.17	430	−0.29	220	1.95
3	Glycerol	+0.18	380	−0.32	160	2.25
4	Xylitol	+0.21	250	−0.38	65	3.85

contributor to the reduction in the electrocatalytic activity [10, 11]. Figure 5A shows the CVs for a PPy/MOH/Pd electrode in 1 M KOH/1 M CH_3OH in the (1) −1.1 to +0.2 V, (2) −1.1 to +0.4 V, (3) −1.1 to +0.6 V and (4) −1.1 to +0.8 V ranges. In all the CVs, a forward sweep of the anodic oxidation peak appeared between −0.6 and −0.07 V, with vertex potential at −0.2 V. During the reverse sweep, the secondary oxidation peak appeared between −0.15 and −0.6 V (Ep = −0.34 V). Upon increasing the forward sweep potential from +0.2 to +0.4 V, the comparatively inferior peak current (j_b) response of 40 mA cm^{-2} was observed in the reverse sweep. As the sweep potential was further increased up to +0.6 and +0.8 V, their corresponding O^b peak current decreased significantly and the oxidation potential also shifted to a lower potential.

The effect of the catalyst in removing the poisonous intermediates was analyzed using the j_f/j_b ratio (Table 2). In the case of MOR, the j_f/j_b ratio of 2.43 was observed as the upper sweep potential increased to +0.2 V. As the upper sweep potential increased to +0.4 V, a smaller amount of intermediate was oxidized, as was indicated by the decreased O^b current. With a further increase in potential to +0.6 V (and j_f/j_b ratio of 9.43), almost 50 % of the intermediates were oxidized. As the upper sweep potential reached +0.8 V (j_f/j_b is 33), the O^b peak current was drastically decreased and almost 96 % of the intermediates were oxidized (Table 3). In the forward sweep, the anodic oxidation peak appeared in the same position of

Table 3 The j_f/j_b ratios for the electrooxidation of various alcohols over a PPy/MOH/Pd nanocomposite electrode in alkaline medium at various scanning potentials

S. no.	Alcohol	j_f/j_b ratio				
		−1.1 to +0.2 V	−1.1 to +0.4 V	−1.1 to +0.6 V	−1.1 to +0.8 V	−1.1 to +1.0 V
1	Methanol	2.43	2.6	9.43	33.00	–
2	Ethylene glycol	1.95	2.2	4.25	14.17	85
3	Glycerol	2.25	3.8	7.60	25.33	380
4	Xylitol	3.85	7.4	7.62	16.66	25

(Ep) −0.2 V, and during the reverse sweep, the peaks were shifted toward a lower potential with reduced peak current. This indicates the gradual removal of poisoning intermediates formed during the forward sweep. Similar voltammetric responses were observed in EOR, the glycerol oxidation reaction (GOR), and XOR (Fig. 5B–D). As the upper peak potential increased to +1.0 V, the oxidation of intermediates was maximized. In addition, a new forward oxidation peak (O^{f2}) was obtained at +0.5 V for EOR, GOR, and XOR. The appearance of O^{f2} was associated with the oxidation of the intermediates formed at O^{f1}.

3.5 Mechanism for the oxidative removal of intermediates at higher potential

In this section, we discuss the oxidation of poisoning intermediates formed during MOR at higher potentials on the PPy/MOH/Pd electrode. In MOR, the unreacted $Pd_2(CO)_{ads}$ may act as a poisoning intermediate (Eq. 10) [10]. These intermediates are strongly bound to the surface of the catalyst. The complete removal of intermediates may not be possible until the forward potential of Ep = +0.2 V is reached, because active oxygen is less available in this region. The oxidation of these intermediates requires a high availability of active oxygen. The highly active oxygen becomes available at the potential which OER occurs, i.e., above +0.2 V. OER begins at the electrode surface, and the formed oxygen is highly energetic and active. Active oxygen oxidizes the poisoning intermediates adsorbed on the electrode surface, as was confirmed from the diminishing O^b peak current in MOR and the formation of O^{f2} in EOR and GOR. In addition, the O^b peak is shifted to a lower potential. Increasing the potential in the forward sweeps accelerates the conversion of Pd to PdO, hence shifting the O^b to a lower potential region [16, 24, 25].

The formation of active oxygen on the electrode surface is explained by the following equations [17, 19, 31]

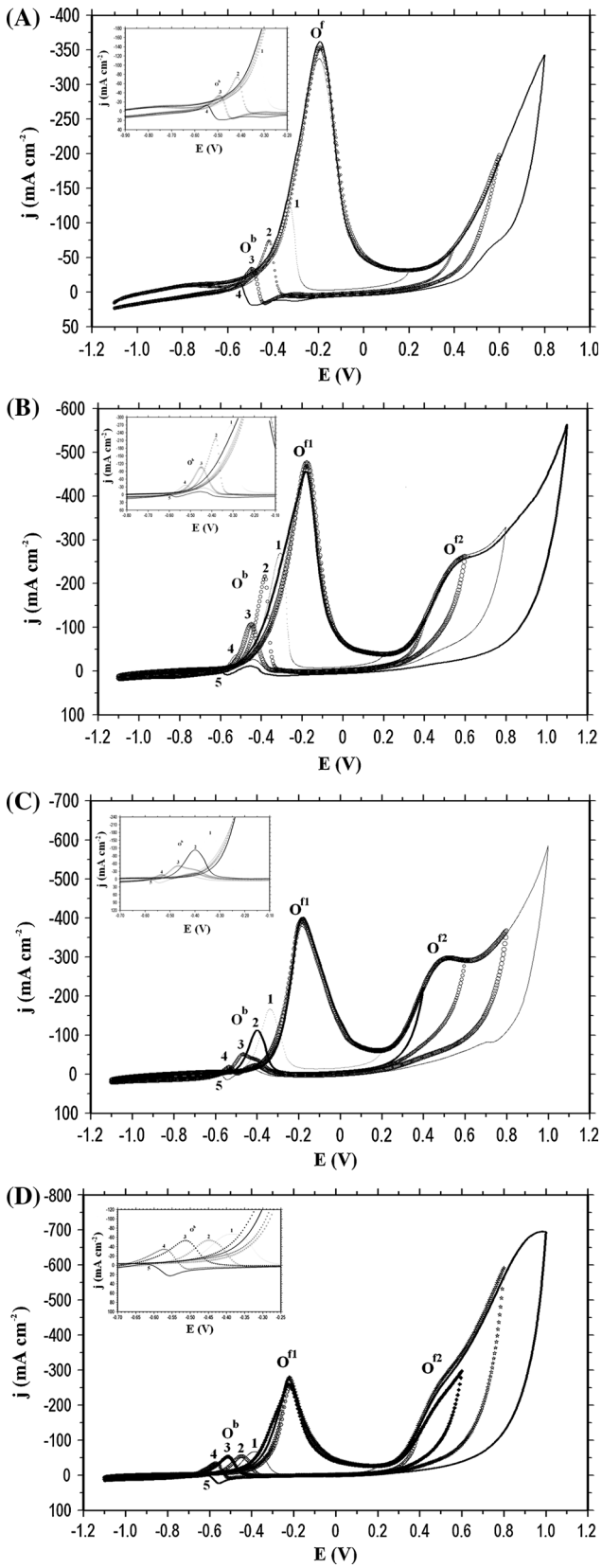

◀**Fig. 5** CVs of the electrooxidation of **A** methanol, **B** ethylene glycol (EG), **C** glycerol, and **D** xylitol over a PPy/MOH/Pd nanocomposite electrode with sweeping potential ranging from −1.1 to (1) +0.2 V, (2) +0.4 V, (3) +0.6 V, (4) +0.8 V, and (5) +1.0 V

$$Pd/MnOOH + OH^- \leftrightarrow Pd/MnO_2 + H_2O \quad (13)$$

$$Pd/MnO_2 + OH^- \rightarrow Pd/MnO_2—(OH^-)_{ads} \quad (14)$$

$$Pd/MnO_2—(OH^-)_{ads} \rightarrow Pd/MnOOH + (O)_{ads} \quad (15)$$

$$MnO_2/Pd—CO_{ads} + OH^- \rightarrow Pd/MnOOH + CO_2 \quad (16)$$

The surface-adsorbed hydroxide ions on the catalytic electrode are represented by "$(OH)_{ads}$" in the above equations. During the electrochemical sweep, the surface-adsorbed hydroxide ions produced active oxygen ions through OER (Eqs. 13–15), and the oxygen, thereby produced was highly energetic and active. The active oxygen reacted with the intermediates thereby removed through oxidation (Eq. 6). In addition, the low–temperature preparation of the manganese oxide used in this study induced a high probability of surface defects. These surface defects at the electrode–electrolyte interface may have helped extract the active oxygen from the electrolyte through OER. The proposed reaction scheme (Scheme 1) for MOR over the PPy/MOH/Pd nanocomposite electrode reveals the catalytic involvement of manganese oxide in the reaction. Our study results support the catalytic role played by manganese oxide in the electrooxidation reaction, which was enabled by the active oxygen supplied by the reversible redox system of MOH ($Mn^{4+/3+}$) [17, 19]. The catalytic involvement of the MOH support material was vital as it played two important roles: acting as a support for noble metals and as a co-catalyst.

Chronoamperometry was conducted to test the electrocatalytic stability of the PPy/MOH/Pd nanocomposite electrode, the overall stability decreasing in the order of glycerol > methanol > EG = xylitol (Fig. 6A). The interference of the poisoning intermediates was further evaluated by continuous CV cycling, during which a decreased peak current of about 5–7 % was observed over 500 cycles, demonstrating the stability of the electrode over repeated cycles (Fig. 6B). This stability was verified by varying the scan rate in EOR (Fig. 7). The relationship between peak current and the square root of the scan rate (Fig. 7 inset) demonstrates that the electrode was highly surface-controlled. Mechanistic investigations of the electrooxidation of alcohols and analysis of the intermediates are presently underway.

Scheme 1 Proposed mechanism for the electrooxidation of methanol over a PPy/MOH/Pd nanocomposite electrode

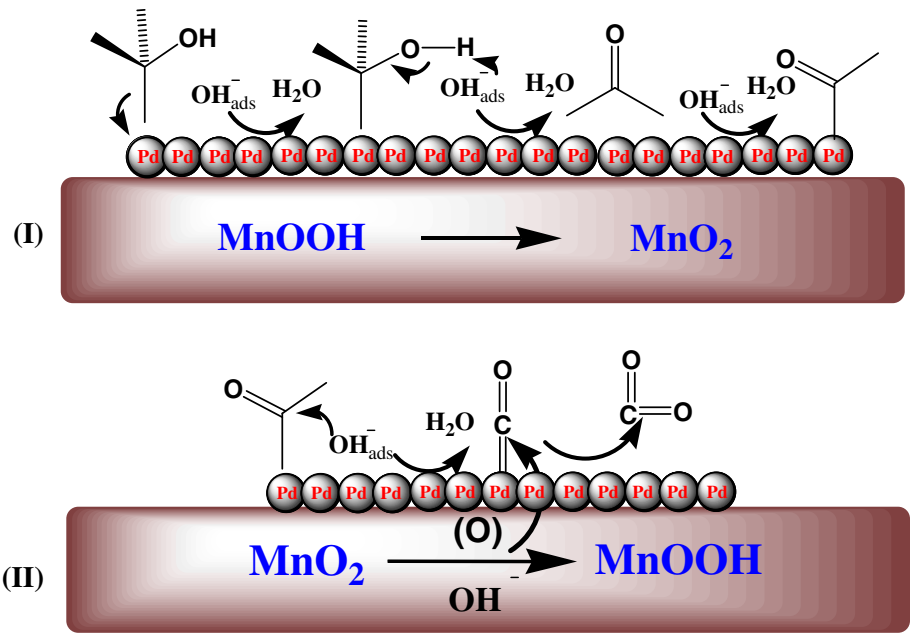

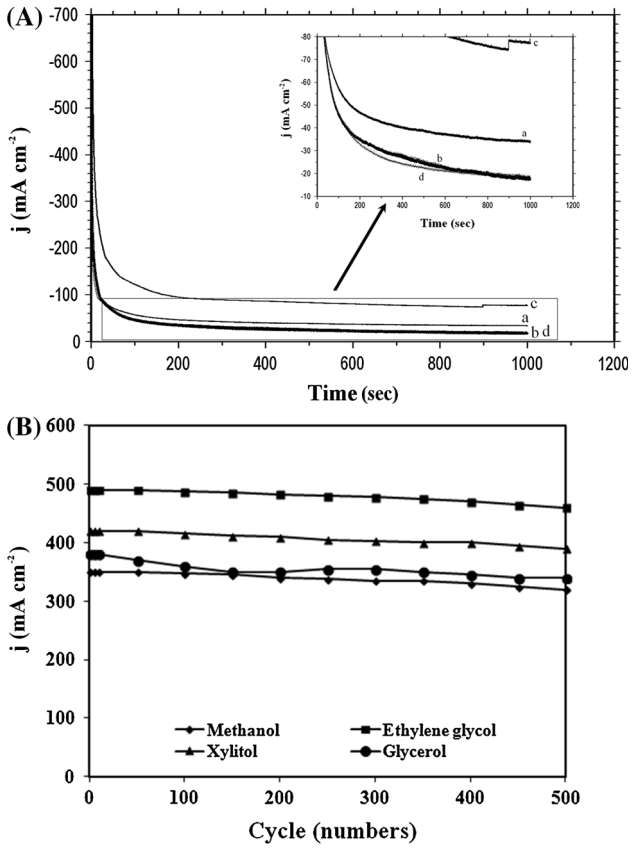

Fig. 6 **A** Chronoamperograms obtained for the electrooxidation of (*a*) methanol, (*b*) ethylene glycol (EG), (*c*) glycerol, and (*d*) xylitol over a PPy/MOH/Pd nanocomposite electrode; and **B** stability of the PPy/MOH/Pd nanocomposite electrode for the alcohol electrooxidation over repeated cycles

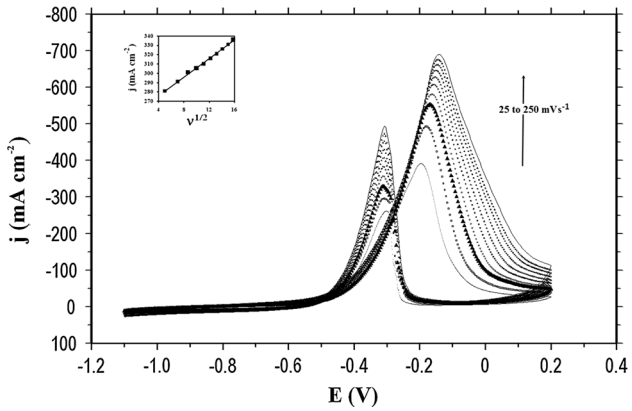

Fig. 7 CVs for the electrooxidation of EG at various scan rates (25–250 mV s^{-1}) in 1 M KOH/1 M EG over a PPy/MOH/Pd nanocomposite electrode. Inset: peak current versus square root of the scan rate

4 Conclusion

The current study addresses the electrocatalytic oxidation of methanol, EG, glycerol, and xylitol over a noble metal nanoparticulate ternary catalyst composed of Pd and a PPy/MOH nanocomposite. The combination of Pd nanoparticles and the PPy/MOH composite yielded an efficient electrocatalyst for the alcohol electrooxidation reaction. A small quantity of 5 wt% Pd-loaded PPy/MOH nanocomposite electrocatalyst exhibited excellent electrocatalytic activity. The manganese-nitrogen interaction creates an

active site, results enhanced electrochemical performance was observed. The polymer (PPy) provided an excellent conductive networking and PPy/MOH) acts as co-catalyst for the oxidation of intermediates. In summary, PPy/MOH behaved as an active support material for the Pd catalyst in the alcohol electrooxidation reaction in alkaline media. It is believed that this efficient and economic catalyst could facilitate the scale up and commercialization of DAFCs for practical application.

Acknowledgments The research was supported by the Basic Science Research program through the National Research Foundation of Korea (NRF) funded by the Ministry of Education, Science and Technology (2011–0010538).

References

1. Bianchini C, Shen PK (2009) Palladium-based electrocatalysts for alcohol oxidation in half cells and in direct alcohol fuel cells. Chem Rev 109:4183–4206
2. Yu EH, Krewer U, Scott K (2010) Principles and materials aspects of direct alkaline fuel cells. Energies 3:1499–1528
3. Wang YJ, Wilkinson DP, Zhang J (2011) Noncarbon support materials for polymer electrolyte membrane fuel cell electrocatalysts. Chem Rev 111:7625–7651
4. Brouzgou A, Song SQ, Tsiakaras P (2012) Low and non platinum electrocatalyst for PEMFCs: current status, challenges and prospects. Appl Catal B Environ 127:371–388
5. Brouzgou A, Podias A, Tsiakaras P (2013) PEMFCs and AEMFCs directly fed with ethanol: a current status comparative review. J Appl Electrochem 43(2):119–136
6. Serov A, Kwak C (2010) Recent achievements in direct ethylene glycol fuel cells (DEGFC). Appl Catal B Environ 97:1–12
7. Xu C, Liu Y, Yuan D (2007) Pt and Pd supported on carbon microspheres for alcohol electrooxidation in alkaline media. Int J Electrochem Sci 2:674–680
8. Kohlmuller H (1976) Anodic oxidation of ethylene glycol with noble metal alloy catalysts. J Power Sources 1:249–256
9. Janssen MMP, Moolhuysen J (1976) Binary systems of platinum and a second metal as oxidation catalysts for methanol fuel cell. Electrochim Acta 21:869–878
10. Nishimura K, Kunimatsu K, Enyo M (1989) Electrocatalysis on Pd + Au alloy electrodes: part III. IR spectroscopic studies on the surface species derived from CO and CH_3OH in NaOH solution. J Electroanal Chem 260:167–179
11. Manaoharan R, Prabhuram J (2001) Possibilities of prevention of formation of poisoning species on direct methanol fuel cell anodes. J Power Sources 96:220–225
12. Musthafa OTM, Sampath S (2008) High performance platinized titanium nitride catalyst for methanol oxidation. Chem Commun 7:67–69
13. Jeon MK, Daimon H, Lee KR, Nakahara A, Woo SI (2007) CO tolerant Pt/WC methanol electro-oxidation catalyst. Electrochem Commun 9:2692–2695
14. Yan Z, Zhang M, Xie J, Shen PK (2012) Vanadium carbide and graphite promoted Pd electrocatalyst for ethanol oxidation in alkaline media. J Power Sources 243:336–342
15. Pandey RK, Lakshminarayanan V (2009) Electro-oxidation of formic acid, methanol and ethanol on electrodeposited Pd-Polyaniline nanofiber films in acidic and alkaline medium. J Phys Chem C 113:21596–21603
16. Kannan R, Karunakaran K, Vasanthkumar S (2013) Poly(aniline)/MnO_2 supported palladium-a facile nanocatalyst for the electrooxidation of methanol. Mater Focus 2:267–271
17. Xu C, Tian Z, Shen PK, Jiang SP (2008) Oxide (CeO_2, NiO, Co_3O_4 and Mn_3O_4)-promoted Pd/C electrocatalysts for alcohol electrooxidation in alkaline media. Electrochim Acta 53:2610–2618
18. Xu MW, Gao GY, Zhou WJ, Zhang KF, Li HL (2008) Novel Pd/β-MnO_2 nanotubes composites as catalysts for methanol oxidation in alkaline solution. J Power Sources 175:217–220
19. Deab MSE (2011) Platinum nanoparticles–manganese oxide nanorods as novel binary catalysts for formic acid oxidation. J Adv Res 3:65–71
20. Kannan R, Karunakaran K, Vasanthkumar S (2011) PdNi-coated manganite nanorods as catalyst for electrooxidation of methanol in alkaline medium. Appl Nanosci 2:149–155
21. Kannan R, Karunakaran K, Vasanthkumar S (2012) PdNi-decorated manganite nanocatalyst for electrooxidation of ethylene glycol in alkaline medium. Ionics 18:803–809
22. Kannan R, Karunakaran K, Vasanthkumar S (2012) Nanostructured OMO type manganese oxide – as novel support for palladium towards electrooxidation of methanol and ethylene glycol. J New Mater Electrochem Syst 15:249–254
23. Scibioh MA, Kim SK, Cho EA, Lim TH, Hong SA, Ha HY (2008) Pt-CeO_2/C anode catalyst for direct methanol fuel cells. Appl Catal B Environ 84:773–782
24. Wen Q, Wang S, Yan J, Cong L, Pan Z, Ren Y, Fan Z (2012) MnO_2-graphene hybrid as an alternative cathodic catalyst to platinum in microbial fuel cells. J Power Sources 216:187–191
25. Yang X, Wang X, Zhang G, Zheng J, Wang T, Liu X, Shu C, Jiang L, Wang C (2012) Enhanced electrocatalytic performance for methanol oxidation of Pt nanoparticles on Mn_3O_4-modified multi-walled carbon nanotubes. Int J Hydrog Energy 37:11167–11175
26. Li L, Scott K, Yu EH (2013) A direct glucose alkaline fuel cell using MnO_2-carbon nanocomposite supported gold catalyst for anode glucose oxidation. J Power Sources 221:1–5
27. Wei L, Fan YJ, Ma JH, Tao LH, Wang RX, Zhong JP, Wang H (2013) Highly dispersed Pt nanoparticles supported on manganese oxide-poly(3,4-ethylenedioxythiophene)-carbon nanotubes composite for enhanced methanol electrooxidation. J Power Sources 238:157–164
28. Gharibi H, Kakaei K, Zhiani M (2010) Platinum nanoparticles supported by a Vulcan XC-72 and PANI doped with trifluoromethane sulfonic acid substrate as a new electrocatalyst for direct methanol fuel cells. J Phys Chem 114:5233–5240
29. Liang ZX, Zhao TS, Xu JB, Zhu LD (2009) Mechanism study of the ethanol oxidation on palladium in alkaline media. Electrochim Acta 54:2203–2208
30. Pattabiraman R (1997) Electrochemical investigations on carbon supported palladium catalysts. Appl Catal A Gen 153:9–20
31. Deab MSE, Awad MI, Mohammad AM, Ohsaka T (2007) Enhanced water electrolysis: electrocatalytic generation of oxygen gas at manganese oxide nanorods modified electrodes. Electrochem Commun 9:2082–2087